Communications in Physics, Vol. 30, No. 4 (2020), pp. 409-416
DOI:10.15625/0868-3166/30/4/14964

FACILE SYNTHESIS AND CHARACTERIZATION OF THE REDUCED GRAPHENE OXIDE/Co_3O_4 NANOCOMPOSITE FOR CAPACITIVE APPLICATION*

PHAM THI NAM[1,2], NGUYEN THI THOM[1], NGUYEN THI THU TRANG[1], DINH THI MAI THANH[1,3], VO THI KIEU ANH[1], ANH SON NGUYEN[1] AND TRAN DAI LAM[1,2,†]

[1]*Institute for Tropical Technology, Vietnam Academy of Science and Technology, 18 Hoang Quoc Viet, Cau Giay, Ha Noi, Vietnam*

[2]*Graduate University of Science and Technology, Vietnam Academy of Science and Technology, 18 Hoang Quoc Viet, Cau Giay, Ha Noi, Vietnam*

[3]*University of Science and Technology of Hanoi, Vietnam Academy of Science and Technology, 18 Hoang Quoc Viet, Cau Giay, Ha Noi, Vietnam*

[†]*E-mail:* tdlam@itt.vast.vn

Received 07 April 2020
Accepted for publication 04 December 2020
Published 16 December 2020

Abstract. *This work suggests a simple strategy to synthesize reduced graphene oxide/Co_3O_4 (rGO/Co_3O_4) from graphene oxide (GO) and $Co(CH_3COO)_2$ precursor using ultrasonic method. The synthesized rGO/CO_3O_4 was thoroughly characterized by SEM/EDX, XRD, FTIR and BET. The obtained results indicate the presence of well-crystalized Co_3O_4 nanoparticles onto the rGO nanosheets in the lamellar structure of rGO/Co_3O_4. Despite slight decrease in BET specific surface area (from 389.9 m2/g of rGO to 218.7 m^2/g of rGO/CO_3O_4), CV measurements illustrate an improved specific capacitance (95.8 F/g at 50 mV/s) with redox properties for the rGO/Co_3O_4 electrode. The synthesized composites are expected to be a potential electrode candidate in supercapacitor as well as in hybrid deionized capacitive system for the desalination purpose.*

Keywords: reduced graphene oxide (rGO); Co_3O_4; capacitive application.

Classification numbers: 84.32.Tt; 81.05.Ue; 72.80.Tm.

*This paper is dedicated to the 40th anniversary of Institute for Tropical Technology

I. INTRODUCTION

Graphene is a well-known superior material with two-dimensional monolayer of carbon atoms due to its excellent physical and chemical properties such as good mechanical stability, super thermal conductivity, large surface area and high carrier mobility. Therefore, it provided enormous advances in various fields, such as catalysts, biomedicine, sensors, composite materials, solar cells, electrical and energy equipment, especially supercapacitors [1–4]. In recent years, many studies have been examined on specific surface area, electrical properties and stability of chemical as well as thermal of graphene-based supercapacitor [5–16].

Although being outstanding candidate, the supercapacitors based on graphene currently presented the charging time and lifetime that is not long enough to the most practical capacitive applications. One feasible solution to overcome this issue is to develop the pseudo-capacitors that can transfer and store energy through redox reactions. They provided to high specific capacitance with improved energy density [17]. For reaching this goal, different transition metal oxides such as NiO, MnO_2, Fe2O_3, and Co_3O_4 are exploited as great potential materials for the pseudo-capacitor electrode [17–20]. These metal oxides alone give a large specific capacitance, but they present a poor electrical conductivity that induces low power density and poor rate capability. For obtaining high-performance supercapacitor with both high energy density and power density, the combination between rGO and transition metal oxides is an interesting topic to investigate. Recently, much attention is being focused on rGO/Co_3O_4 due to very high theoretical capacity of (3580 F/g) and remarkable reversibility of Co_3O_4 [21]. Feng Du *et al.* fabricated the composite of Co_3O_4RGO with the specific capacitance of 894 F/g which is higher than that of pure Co_3O_4 (300 F/g). The electrode of Co_3O_4RGO showed a long-term ability after 3000 cycles [22]. It can see that the super performance of the composite electrode is attributed to the synergistic effects of small size and good redox activity of the Co_3O_4 particles combined with high electrical conductivity of the rGO [23].

In this work, the simple ultrasonic method to synthesize rGO/Co_3O_4 from graphene oxide (GO) and $Co(CH_3COO)_2$ was reported. The rGO/Co_3O_4 nan˚Composite was then characterized by Scanning electron microscopy (SEM), Energy dispersive rayon-X spectroscopy (EDX), X-ray diffraction (XRD) and Fourier-transform infrared spectroscopy (FTIR). Finally, some main parameters of electrochemical capacitors of rGO/Co_3O_4 were studied by using N_2 isothermal adsorption methods and Cyclic voltammetry.

II. MATERIALS AND METHODS

II.1. Materials and sample preparation

GO powder with a lateral size of about 45 nm (pure $>$ 99%) was purchased from Sigma-Aldrich (796034_ALDRICH). Acetonitrile (CH_3CN), tetraethylammonium tetrafluoroborate (TEABF4) were supplied by Merck. $Co(CH_3COO)_2$, H_2O_2 and NH_3 solutions were analytical chemicals (China), and were used as received.

0.15 g of GO is dispersed in 100 mL distilled water using an ultrasonication for 30 min. Then, 10 mL of 15 g/L $Co(CH_3COO)_2$ is added into the GO solution. This mixture is under ultrasound for 30 min. NH4OH solution is added to the above mixture to adjust pH solution of 8 or 9, and then 15 mL H_2O_2 30% is added. The resulting mixture is ultrasonically dispersed for

15 mins at 45°C. The rGO/Co_3O_4 is obtained by filtration of precipitate with distilled water, dried and incubated for 1 hour at 650°C in N_2.

II.2. Analytical methods

The characterization of rGO and rGO/Co_3O_4 was analyzed using SEM, EDX (JSM-6510, JEOL), TEM (JEM1010), XRD (D5005 Bruker, Siemens) and FT-IR (iS10, Nicolet). The cyclic voltammetry (CV) measurements were realized using VSP-300 potentiostat (Bio-lig) with three-electrode system which contains Ag/AgCl reference electrode, platinum grid and analyzed materials used as counter and working electrode, respectively. For the electrochemical specimens, rGO and rGO/Co_3O_4 powders were mixed with polytetrafluoroethylene (PTFE, used as binder) and carbon black (CB, used as conducting agent) at a weight ratio of 85:10:5. The mixtures were then molded by hydraulic pressing Specac to form a cyclindical tables with a diameter of 1.2 cm and a thickness of 3 mm. The prepared electrodes were dried in an oven for 4 h at 140°C. For controlling the working surface of electrode, they were coved by epoxy resin. All electrochemical measurements were performed in an acetonitrile (CH_3CN) solution containing 0.1 M tetraethylammonium tetrafluoroborate (TEABF4) over a voltage range from -0.1 V to $+0.6$ V at scan rate of 50 mV/s. From the CV curves, the specific capacitance (C, F/g) was calculated according to the following formule:

$$C = \frac{I.\Delta t}{m\Delta E} = \frac{Q}{m.\Delta E}, \tag{1}$$

where I, Δt, m and ΔE are the current density (A), the time (s) of the charge or discharge process, the sample mass (g) and the board potential (V), relatively.

III. RESULTS AND DISCUSSION

The morphology of synthesized rGO and rGO/Co_3O_4 is studied by SEM technique. Figure 1a presents a multi-layer structure of the as-synthesized rGO, in which the nanosheets of rGO have an ultrathin thickness (some nm) and a lateral dimension ranged from hundreds of nanometers to several micrometers. This observation is similar to that in literature [24]. Due to the van der Waal's interactions, the rGO nanosheets are randomly aggregated and rippled with each other as crumpled silk veil waves [25]. Regarding rGO/Co_3O_4, the characteristic lamellar structure of rGO is still observed in Figure 1b. The high-magnification SEM images of rGO/Co_3O_4 illustrate the presence of Co_3O_4 nanoparticles that are firmly anchored onto the wrinkled graphene sheets.

To confirm the presence of Co_3O_4 into the rGO/Co_3O_4 composite, TEM analysis was used. The TEM images of rGO and rGO/Co_3O_4 show the layers of graphene (Fig. 2). It can be seen clearly that the presence of Co_3O_4 particles into the layers of graphene (see Fig. 2b).

Figure 3 presents the energy dispersive X-ray spectroscopy (EDX) spectra of rGO and rGO/Co_3O_4 powders. For EDX spectrum of free standing rGO, only two elemental peaks of C and O are displayed, while an additional peak corresponding to Co can be seen on rGO/Co_3O_4 spectrum. The atomic and weight percentages of C, O and Co in rGO and rGO/Co_3O_4 obtained from EDX analysis are fully given in Table 1 (Atomic % is the % as a function of the number of atoms whereas wt % would be % as a function of weight). It can be seen from this table that the weight % of Co in rGO/Co_3O_4 composition was 5.40%. Due to the presence of Co_3O_4, the atomic content of O in rGO/Co_3O_4 (12.44%) was higher than that in rGO (11.63%). The slight decrease of C:O ratio in rGO/Co_3O_4 (6.94) compared to that of rGO (7.60) can be logically expected.

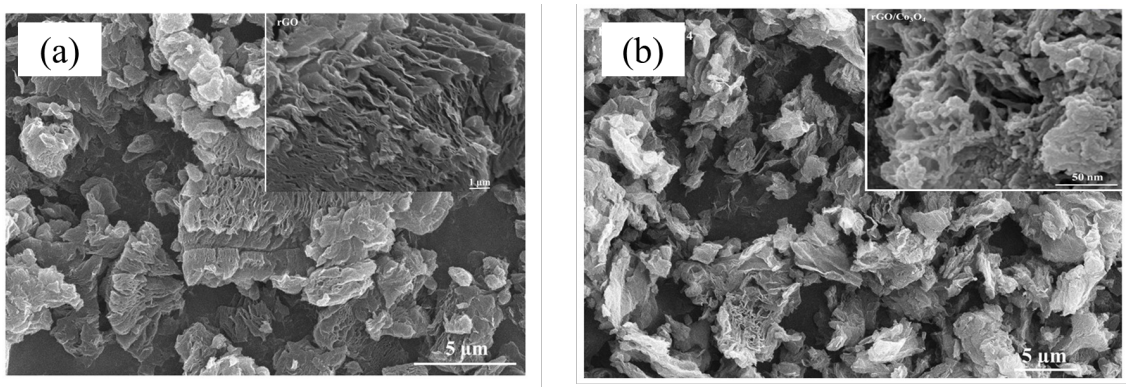

Fig. 1. SEM micrographs of synthesized rGO (a) and rGO/Co_3O_4 (b).

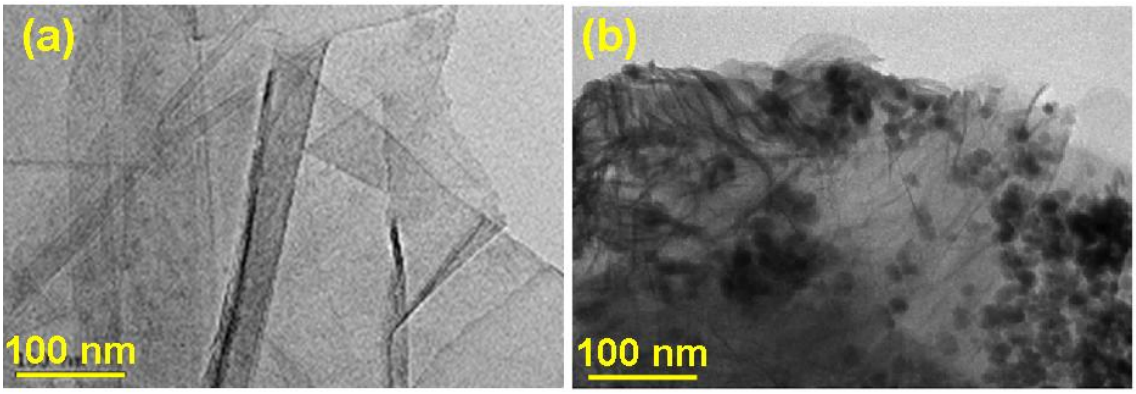

Fig. 2. TEM images of synthesized rGO (a) and rGO/Co_3O_4 (b).

Table 1. EDX elemental analysis of rGO and rGO/Co_3O_4 composites.

Samples	% weight			% atomic			Ratio
	C	O	Co	C	O	Co	C/O
rGO	85.07	14.93	-	88.37	11.63	-	7.60
rGO/Co_3O_4	79.35	15.25	5.40	86.36	12.44	1.20	6.94

To investigate the crystal structure of rGO and rGO/Co_3O_4 powders, X-Ray diffraction (XRD) was used (Fig. 4). As for rGO nanosheets, the typical diffraction peak is observed at $2\theta = 25.8^{\circ}$, which can be attributed to (002) crystal plane [26] (denoted as phase #1). It should be noted that high-intensity peak reveals a good crystallinity of synthesized rGO sheets. Regarding rGO/Co_3O_4, the XRD pattern shows the characteristic diffraction peaks of both Co_3O_4 and rGO phases. Namely, the sharp peaks at $2\theta = 19^{\circ}$, 31.1°, 36.6°, 44.9°, 58.5° and 65°, corresponding to (111), (220), (311), (400), (422) and (511) crystal planes of Co_3O_4 phase respectively are recorded (phase #2). According to the JCPDS No.42-1467, these peaks illustrated that the

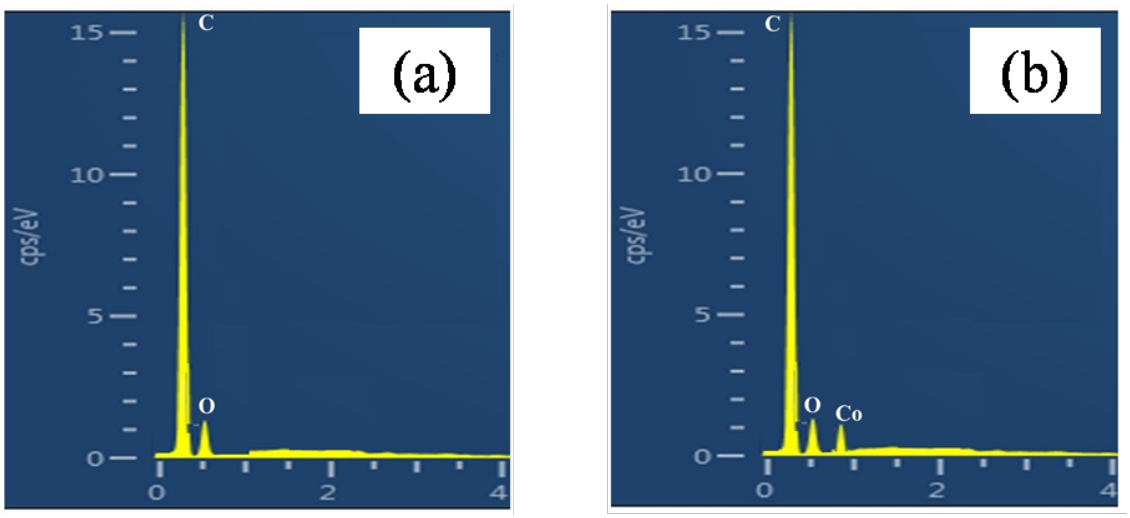

Fig. 3. EDX analysis of rGO (a) and rGO/Co_3O_4 (b).

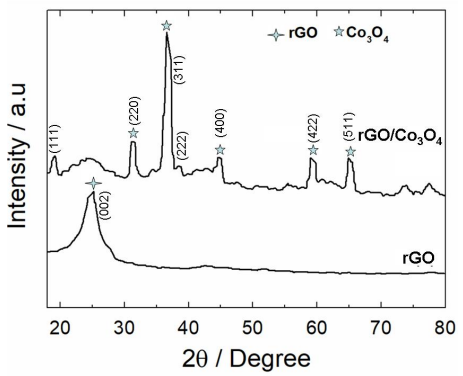

Fig. 4. XRD pattern of synthesized rGO and rGO/Co_3O_4.

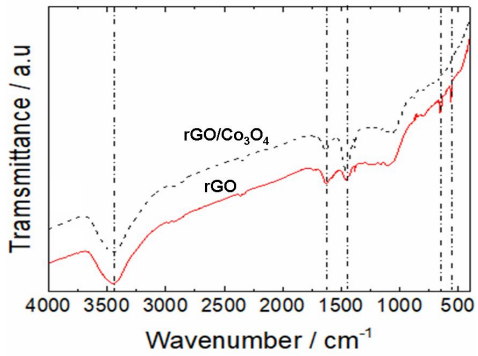

Fig. 5. FTIR spectra of rGO and rGO/Co_3O_4.

crystalline structure of Co_3O_4 was standard face-centered cubic [27]. Meanwhile, a broad peak centered at $2\theta = 25.8^{\circ}$ in the XRD pattern is clearly assigned to rGO phase. Briefly, the fact that XRD pattern changes notably with the appearance of a new phase of Co_3O_4 when maintaining the characteristic peak of rGO demonstrates that the synthesized rGO/Co_3O_4 contains both stacked rGO sheets and well-crystalized Co_3O_4 nanoparticles.

The FT-IR spectra of the rGO, and rGO/Co_3O_4 composite (Fig. 5) indicate that the broad absorption peak at 3455 cm^{-1} corresponds to -OH group. Quite strong peaks at 1460 cm^{-1} and 1640 cm^{-1} are commonly attributed to –OH bending vibration of absorbed water molecules and contribution from skeletal vibration of aromatic $C = C(sp^2)$ respectively [28, 29]. The peaks at 650 and 565 cm^{-1} were assigned to Co-O vibrations of cobalt oxide nanoparticles [30]. Therefore, XRD pattern and FTIR spectra have unambiguously confirmed the existence of Co_3O_4 in the composition of rGO/Co_3O_4.

Since gas adsorption is a typically method for the characterization of porous structure, therefore, to study the porous structure of as-synthesized rGO and rGO/Co_3O_4, the nitrogen adsorption-desorption technique was used. Fig. 6 illustrates that the N_2 isothermal adsorption curves of both samples have a similar shape and the adsorption yields a type III isotherm (IUPAC definition), according to which it has no identifiable monolayer formation. In addition, it demonstrates weak adsorbent-adsorbate interactions, which induce the clustered adsorbed molecules around the most suitable area of macro-porous and nonporous solids. Indeed, the curves in the low P/P° range (0.0 to 0.1) slightly increased as a function of relative pressure, which can be attributed to relatively weak adsorbent-adsorbate. At higher P/P° (0.1 to 0.4), molecular clustering is followed by pore/mesopore filling. The obtained results propose the isothermal adsorption behavior of layer structure of rGO and rGO/Co_3O_4 composites. The BET surface areas are calculated from N_2 adsorption isotherm and summarized in Table 2. These data are in good agreement with the SEM micrographs as shown above and comparable to those reported in the literature [31]. It should also be noted that calculated BET specific surface area for rGO/Co_3O_4 is less than that for rGO (218.7 m^2/g compared to 389.9 m^2/g) due the presence of Co_3O_4 nanoparticles filling in the pores/mesopores of the structure of rGO and thus leading to decrease in capillary volume of rGO/Co_3O_4.

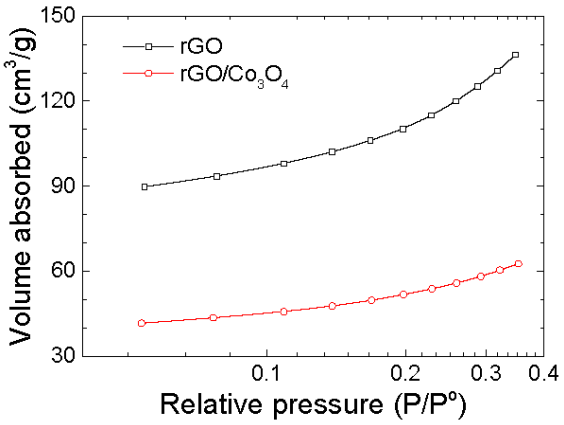

Fig. 6. N_2 isothermal adsorption curves at 77.3 K of rGO and rGO/Co_3O_4.

Table 2. BET parameters calculated from N_2 isothermal adsorption curves for rGO and rGO/Co_3O_4.

Parameters	rGO	rGO/Co_3O_4
SBET (m^2/g)	389.9	218.7
Pore volume (cm^3/g)	0.02	0.01
Total pore volume (cm^3/g)	0.17	0.07
Average pore diameter (nm)	2.29	2.34

The CV technique was performed to determine the electrochemical properties of the synthesized materials at a scan rate of 50 mV/s in potential range from - 0.1 V to 0.6 V. Fig. 7 displays that the CV curves of rGO and rGO/Co_3O_4 have a rectangular shape which describe to charge/discharge curve of supercapacitor. Due to the presence of Co_3O_4 onto rGO plate which introduces the pseudo-capacitance, the area of the CV curve for rGO/Co_3O_4 material is larger than that for rGO. In addition, this curve also shows 2 redox peaks at 0.10 V and 0.35 V corresponding to conversion between different cobalt oxidation states, as follows [32]:

$$Co_3O_4 + OH^- + H_2O \leftrightarrow 3CoOOH + e^- \quad (2)$$

$$CoOOH + OH^- \leftrightarrow CoO_2 + H_2O + e^- \quad (3)$$

From CV curves in Fig. 6, the specific capacitances of rGO and rGO/Co_3O_4 were calculated according to the equation (1) (Table 3). It shows that the specific capacitances obtained for rGO/Co_3O_4 is about 1.5 times higher than that for free standing rGO (free-Co_3O_4), 95.8 F/g and 62.5 F/g, respectively. It can be explained by the presence of Co_3O_4 nanoparticles provides the various active redox sites having higher power and energy density and thus leading to better overall electrochemical performance of rGO/Co_3O_4 composites. Although the specific capacitance of the material in this study is lower than in other reports, but also it is still consistent with the previously reported by other authors [5, 21, 24] that the presence of Co_3O_4 has significantly improved the specific capacitance for pure GO.

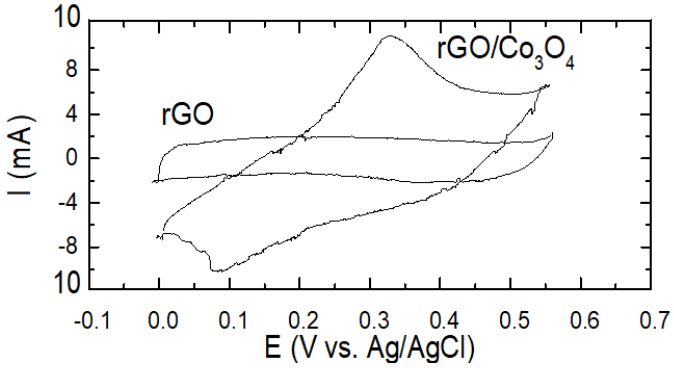

Fig. 7. The CV curves at scan rate of 50 mV/s for rGO and rGO/Co_3O_4.

Table 3. Specific capacitances of rGO and rGO/Co_3O_4 obtained from CV curves.

Parameters	rGO	rGO/Co_3O_4
Mass (g)	0.20	0.20
C (F/g)	62.5	95.8

IV. CONCLUSION

In summary, the rGO/Co_3O_4 nanocomposite was synthesized from GO and $(COOH)_2Co$ precursor by simple ultrasonic method. The nanocomposite was then characterized by using SEM/EDX, XRD, FTIR, N_2 isotherms adsorption and electrochemical techniques. Through these results, the rGO/Co_3O_4 material has multiple layer structure, porous and contains well-crystalized Co_3O_4 nanoparticles onto the rGO nanosheet. The BET surface area of rGO/Co_3O_4 decreased from 389.9 m^2/g to 218.7 m^2/g. However, the specific capacitances of rGO/Co_3O_4 were enhanced, about 1.5 times higher than that of GO. It demonstrates that the proposed synthetic method can be used to obtain rGO/Co_3O_4. Further works of our group are underway to investigate the application of the above synthesized composites as electrode materials in supercapacitor as well as in hybrid capacitive deionization (HCDI) system for the desalination purpose.

ACKNOWLEDGEMENTS

The authors gratefully acknowledge the financial support from National Foundation for Science and Technology Development (NAFOSTED) under grant number 104.03-2018.344 and from Vietnam Academy of Science and Technology (VAST) under grant number NCVCC 13.02/20-20.

REFERENCES

[1] M.C. Nongbe, T. Ekou, L. Ekou, K. B. Yao, E. Le Grognec, F-X. Felpin, *Renew. Energy* **106** (2017)135.
[2] S. Aznar-Cervantes, J. G. Martinez, A. Bernabeu-Esclapez, A. A. Lozano-Perez, L. Meseguer-Olmo, T. F. Otero, J. L, Cenis, *Bioelectro Chemistry* **108** (2016) 36.
[3] S. Goossens, G. Navickaite, C. Monasterio, S. Gupta, J. J. Piqueras, R. Pérez, G. Burwell, I. Nikitskiy, T. Lasanta, T. Galán, E. Puma, A. Centeno, A. Pesquera, A. Zurutuza, G. Konstantatos, F. Koppens, *Nat. Photonics* **11** (2017) 366.
[4] R. Ishikawa, S. Watanabe, S. Yamazaki, T. Oya, N. Tsuboi, *ACS Appl. Energy Mater.* **2** (1) (2019) 171.
[5] H. Yang, S. Kannappan, A.S. Pandian, J-H. Jang, Y.S. Lee, W. Lu, *Nanotechnology* **28** (44) (2017) 445401.
[6] C. Liu, Z. Yu, D. Neff, A. Zhamu and B. Z. Jang, *Nano Lett.* **10** (2010) 4863.
[7] A. K. Geim, K.S. Novoselov,*Nat. Mater.* **6** (2007) 183.
[8] C. Soldano, A. Mahmood, E. Dujardin, *Carbon* **48**(8) (2010) 2127.
[9] M. J. Allen, V. C. Tung, R. B. Kaner, *Chem. Rev.* **110** (1) 132.
[10] D. R. Dreyer, S. Park, C. W. Bielawski, R.S. Ruoff, *Chem. Soc. Rev.* **39** (2010) 228.
[11] G. Shao, Y. Lu, F. Wu, C. Yang, F. Zeng, Q. Wu, *J. Mater. Sci.* **47** (2012) 4400.
[12] Y. Sun, J. Tang, K. Zhang, J. Yuan, J. Li, D-M. Zhu, K. Ozawa, L-C. Qin, *Nanoscale* **9** (2017) 2585.
[13] M. Mooste, E. Kibena-Põldsepp, B.D. Ossonon, D. Bélanger, K. Tammeveski, *Electrochim. Acta* **267** (2018) 246.
[14] R.K. Singh, R. Kumar, D.P. Singh, *RSC. Adv.* **6** (2016) 64993.
[15] L. G. Guex, B. Sacchi, K. F. Peuvot, R. L. Andersson, A. M. Pourrahimi, V. Ström, S. Farris, R. T. Olsson, *Nanoscale* **9** (2017) 9562.
[16] K.K.H. De Silva, H.-H. Huang, R.K. Joshi, M. Yoshimura, *Carbon* **119** (2017) 190.
[17] J. Li, W. Zhao, F. Huang, A. Manivannan, N.Q. Wu, *Nanoscale* **3**(12) (2011) 5103.
[18] V. Subramanian, H. Zhu, R. Vajtai, P.M. Ajayan and B. Wei, *J. Phys. Chem. B* **109**(43) (2005) 20207.
[19] J. Liu, J. Jiang, C. Cheng, H. Li, J. Zhang, H. Gong, H.J. Fan, *Adv. Mater.* **23** (2011) 2076.
[20] A. Abdi, M. Trari, Electrochim. Acta 111 (2013) 869.
[21] Z-S. Wu, Y. Sun, Y-Z. Tan, S. Yang, X. Feng, K. Mullen, *J. Am. Chem. Soc.* **134** (48) (2012) 19532.
[22] Feng Du, Xueqin Zuo, Qun Yang, Guang Li, Zongling Ding, Mingzai Wua, Yongqing Ma, Shaowei Jin, Kerong Zhu, Electrochim. Acta **222** (2016) 976.
[23] Chengcheng Xiang, Ming Li, Mingjia Zhi, Ayyakkannu Manivannan, Nianqiang Wu, *J. Power Sources* **226** (2013) 65e70.
[24] M. Haneef, H. Saleem and A. Habib, *Synth. Met.* **223** (2017) 101.
[25] R. Kumar, H-J. Kim, S. Park, A. Srivastava, I-K. Oh, *Carbon* **79** (2014) 192.
[26] Y. Tang, H. Guo, L. Xiao, S. Yu, N. Gao, Y. Wang, *Colloids and Surfaces A: Physicochem. Eng. Aspects* **424** (2013) 74.
[27] W-Y. Li, L-N. Xu, J. Chen, *Adv. Funct. Mater.* **15**(5) (2005) 851.
[28] S. Wang, Q. Li, M. Chen, W. Pu, Y. Wu, M. Yang, *Electrochim. Acta* **215** (2016) 473.
[29] K. Krishnamoorthy, M. Veerapandian, K. Yun, S.J. Kim, *Carbon* **53** (2013) 38.
[30] S.G. Christoskova, M. Stoyanova, M. Georgieva, D. Mehandjiev, *Mater. Chem. Phys.* **60** (1999) 39.
[31] P.I. Ravikovitch, A.V. Neimark, *Colloids and Surfaces A: Physicochem. Eng. Aspects* **187-188** (2001) 11.
[32] X-C. Dong, H. Xu, X-W. Wang, Y-X. Huang, M.B. Chan-Park, H. Zhang, L-H. Wang, W. Huang, P. Chen, *ACS Nano* **6**(4) (2012) 3206.